Proceeding of the 2004 American Control Conference
Boston, Massachusetts June 30 - July 2, 2004

Control of Hysteresis and Kinematic Error Nonlinearities in Harmonic Drives for High Speed Precision Control Applications

Prasanna S. Gandhi
Department of Mechanical Engineering
Indian Institute of Technology, Bombay
Powai, Mumbai 400 076, INDIA
gandhi@iitb.ac.in

Fathi H. Ghorbel
Department of Mechanical Engineering
Rice University
Houston, TX, USA
ghorbel@rice.edu

Abstract— **Important nonlinear transmission attributes exhibiting coupled dynamics and deteriorating performance of harmonic drive systems include hysteresis and kinematic error. This paper presents control algorithms developed to compensate for hysteresis in the presence of kinematic error (KE) for precision position tracking applications with known smooth load on the output side. A model of hysteresis with a linear flexibility part and nonlinear dissipative part represented by a differential equation is used. The model is integrated with kinematic error model to obtain a set of equations governing system dynamics. First, a singularly perturbed model of the drive is derived from this set of equations. The proposed algorithm is then developed using integral manifold control approach involving slow and fast control terms. A recent result by authors on compensation of kinematic error alone is employed for the same. Simulation results with the proposed algorithms establish its effectiveness.**

Keywords: Harmonic drives, hysteresis, singular perturbations, integral manifold.

I. INTRODUCTION

Harmonic drives are special flexible gear transmission systems developed during the mid-1950s [1] and modified thereafter. The modified version is composed of components identified in Fig. 1(a). The wave generator is a rigid steel core having an elliptical shape with very small eccentricity. It is surrounded by a flexible race ball bearing. The flexible spline (or flexspline) is a thin-walled hollow cup made up of alloy steel. External gear teeth are machined at the open end of this cup while the closed end is connected to the output shaft. The circular spline is a rigid internal gear having two teeth more than those on the flexspline. Upon assembly, the wave generator fits into the open end of the flexspline cup and gives it an elliptical shape at that end. The circular spline teeth then mesh with the flexspline teeth at the major axis of the ellipse defined by the wave generator. A fully assembled harmonic drive is shown in Fig. 1(b). In the most common speed reduction configuration, the wave generator serves as the input port, the flexspline acts as the output port and the circular spline is held immobile. Details of harmonic drive operation can be found in [2], [3].

Construction of harmonic drives with gear meshing at two diametrically opposite ends improves the contact ratio of gear teeth by at least twice that of conventional transmissions. Because of this harmonic drives have higher gear reduction, lower (almost zero) backlash and higher torque-to-weight ratio than the conventional gear drive along with compact design. Hence these drives are popular in many precision positioning applications such as wafer handling machines in semiconductor industry, lens grinding machines, reconnaissance cameras, and military radars. These applications pose a precision position tracking control problem where the output is to follow a desired motion trajectory.

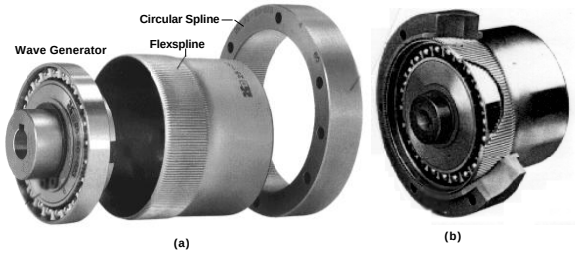

Fig. 1. Harmonic Drive Gear Components (a) and Assembly (b) [4]

Precision positioning performance of harmonic drive systems in these applications is deteriorated by their nonlinear transmission attributes including kinematic error (KE), friction and hysteresis. Research with regard to characterization of the transmission attributes can be found in [5], [6], [7], [8], [2], [9], [10]. Out of these transmission attributes kinematic error, hysteresis display nonlinear coupled nature harmful for high speed precision positioning. The focus of this paper is control of harmonic drive systems in the presence of these nonlinearities. To the best of our knowledge, the literature related to control of harmonic drives [11], [12], [13], [9] have not so far dealt with the control which considers these transmission attributes with their fully coupled nonlinear dynamics. The previous articles [11], [12], [13] mainly address compensation of KE independent of other nonlinearities. However this paper considers hysteresis (arising out of flexibility and friction) dynamics coupled with KE effects. In particular, we develop a position tracking control algorithm to compensate for kinematic error in the presence of nonlinear hysteresis effects. Comparison of simulation results with and without the proposed controller demonstrate its effectiveness. Experimental validation is currently underway.

This paper is organized as follows: Section II presents model of harmonic drive considering nonlinear hysteresis

0-7803-8335-4/04/$17.00 ©2004 AACC

and kinematic error (KE) and time varying output load. This model is used in Section III to derive a singularly perturbed model of harmonic drive. Section IV presents development of the proposed control algorithm to compensate for hysteresis in the presence of kinematic error. Section V presents simulation results and Section VI concludes the paper.

II. MODELING HARMONIC DRIVE HYSTERESIS AND KE

This section presents a model of harmonic drive considering dynamic effects of KE and hysteresis.

Without considering kinematic error and hysteresis nonlinearities, a model of harmonic drive would be given by,

$$\left(J_m N^2 + J_l\right)\ddot{\theta}_l + \left(B_m N^2 + B_l\right)\dot{\theta}_l = \tau_m N, \quad (1)$$

where, $\theta_m = \theta_l N$ and θ_l are the motor and load positions respectively and τ_m is the torque applied to the motor. The parameters are defined and listed in Table II. Experimentally

TABLE I

SYSTEM PARAMETERS USED FOR SIMULATION

Parameter		Numerical Value
Inertia on Motor Side	J_m	$4.5 \times 10^{-4} kgm^2$
Inertia on Load Side	J_l	$5.0 \times 10^{-2} kgm^2$
Damping on Motor Side	B_m	$3.3 \times 10^{-3} Nm - s$
Damping on Load Side	B_l	$5.0 \times 10^{-4} Nm - s$
Gear Ratio	N	50
Hysteresis model	A	$5.5583 \times 10^{3} Nm - s$
Hysteresis model	α	$3.6721 \times 10^{2} rad^{-1}$

obtained waveform of KE is modeled using a general periodic form represented by finite Fourier series as in [8]:

$$KE = \tilde{\theta}_p = \frac{a_0}{2} + \sum_{n=1}^{k} \left[a_n cos(n\theta_m) + b_n sin(n\theta_m)\right], \quad (2)$$

where the Fourier coefficients (a_n, b_n) are obtained using experimental data. Considering only KE, the following model of harmonic drive is obtained using Lagrange formulation [13]:

$$\left(\frac{J_m}{Y_p^2} + J_l\right)\ddot{\theta}_l + \frac{J_m \tilde{\theta}''}{Y_p^4}\dot{\theta}_l^2 + \left(\frac{B_m}{Y_p^2} + B_l\right)\dot{\theta}_l = \frac{\tau_m}{Y_p}. \quad (3)$$

where $Y_p = -\frac{1}{N} + \frac{d\tilde{\theta}_p}{d\theta_m}$, $'$ denotes $\frac{\partial}{\partial \theta_m}$ and other parameters are listed in Table II. Hysteresis in harmonic drive is sandwiched between the input and output dynamics. Recently, harmonic drive hysteresis is modeled accurately using nonlinear flexibility (f) and energy-dissipating (q) parts [10] as follows:

$$H(\theta, q) = f(\theta) + q, \quad (4)$$

where f is spring force, θ is spring deflection, q is additional hysteresis state. Nonlinear flexibility f can be given in terms of polynomial in θ as

$$f(\theta) = m_1\theta + m_2\theta^3 + m_3\theta^5, \quad (5)$$

m_1, m_2, and m_3 are constants. The dissipative part q of hysteresis evolves as per the following differential equation:

$$\frac{dq}{dt} + \alpha\left|\frac{d\theta}{dt}\right| q - A\frac{d\theta}{dt} = 0, \quad (6)$$

where A and α are positive constants. The dissipative part q is in a differential equation form amenable to control. Fig. 2 shows the accurate representation of the multiple experimental hysteresis curves with this model. To simplify development of control algorithm, we use in this paper the same hysteresis model with linear flexibility part instead of the nonlinear one. The simplified hysteresis model h with linear flexibility part is given by

$$H(\theta, q) = K\theta + q, \quad (7)$$

where θ is spring deflection. Though control development is carried out using a simplified linear flexibility part of hysteresis model, simulation results presented in this paper show effectiveness of control using the full nonlinear model presented in [10]. The hysteresis model is integrated (using

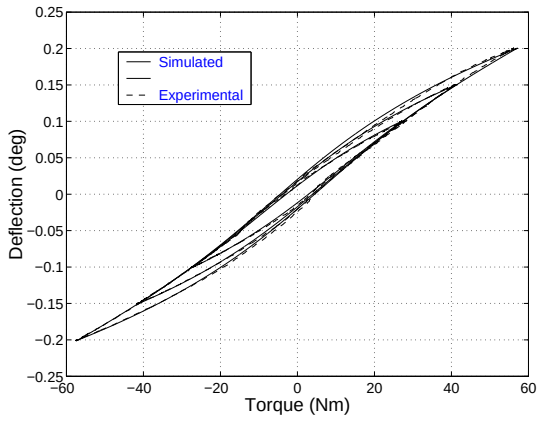

Fig. 2. Experimental and simulated harmonic drive hysteresis curves [10]

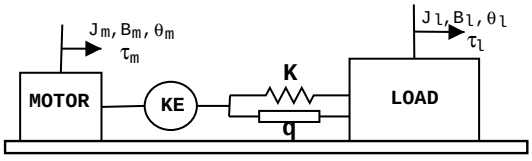

Fig. 3. Schematic representation of harmonic drive system with KE and hysteresis

Newton's method) with the rest of the harmonic drive dynamics with kinematic error $\tilde{\theta}_p$, inertial load and a smooth time varying load torque τ_l (see Fig. 3) as follows:

$$J_m\ddot{\theta}_m - K\left(\theta_l - \frac{\theta_m}{N} + \tilde{\theta}_p\right)Y_p + B_m\dot{\theta}_m - qY_p = \tau_m, \quad (8)$$

$$J_l\ddot{\theta}_l + K\left(\theta_l - \frac{\theta_m}{N} + \tilde{\theta}_p\right) + B_l\dot{\theta}_l + q + \tau_l = 0, \quad (9)$$

$$\dot{q} + \alpha\left|\dot{\theta}_l - \frac{\dot{\theta}_m}{N} + \dot{\tilde{\theta}}_p\right| q - A\left(\dot{\theta}_l - \frac{\dot{\theta}_m}{N} + \dot{\tilde{\theta}}_p\right) = 0, \quad (10)$$

where $Y_p = \frac{1}{N} - \tilde{\theta}_p$ is a new gear reduction ratio varying with position θ_m because of the presence of KE. Notice that the new deflection $\theta = \left(\theta_l - \frac{\theta_m}{N} + \tilde{\theta}_p\right)$ of spring contains the kinematic error term $\tilde{\theta}_p$. From results of [10], [2], it follows that the system of equations (8)-(10) admits a unique solution as long as the input is bounded. This model will be used in the following sections to develop the proposed control algorithms.

III. SINGULARLY PERTURBED MODEL

This section transforms the model of harmonic drive developed above into a singularly perturbed form to be used for subsequent control development. A general nonlinear singularly perturbed system has a standard form [14] given by

$$\dot{\mathbf{x}} = f(t, \mathbf{x}, \mathbf{y}, \epsilon), \quad (11)$$

$$\epsilon\dot{\mathbf{y}} = g(t, \mathbf{x}, \mathbf{y}, \epsilon), \quad (12)$$

where $\mathbf{x}, f \in \mathcal{R}^n$; $\mathbf{y}, g \in \mathcal{R}^m$; $t \in \mathcal{R}$; and ϵ is a small parameter. Before transformation of equations (8)-(10) into the above form, a control law $\tau_m = \tau_{m1} + B_m\dot{\theta}_m$ is used.

Next, following [15] we define spring force as a new fast variable:

$$z = -K\left(\theta_l - \frac{\theta_m}{N} + \tilde{\theta}_p\right). \quad (13)$$

Representing θ_m and its derivatives in terms of z and θ_l gives

$$\theta_m = \left(\frac{z}{K} + \tilde{\theta}_p + \theta_l\right)N, \quad (14)$$

$$\dot{\theta}_m = \frac{1}{Y_p}\left(\frac{\dot{z}}{K} + \dot{\theta}_l\right), \quad (15)$$

$$\ddot{\theta}_m = \frac{1}{Y_p}\left[\frac{\ddot{z}}{K} + \ddot{\theta}_l + \frac{\tilde{\theta}''}{Y_p^2}(\frac{\dot{z}}{K} + \dot{\theta}_l)^2\right]. \quad (16)$$

Substituting for θ_m, $\dot{\theta}_m$, and $\ddot{\theta}_m$ in (8) and (9) above and introducing load position error variable x_1 for trajectory tracking problem, the following equations in the new variables are obtained:

$$\dot{x}_1 = x_2, \quad (17)$$

$$\dot{x}_2 = \frac{1}{J_l}\left(-B_l x_2 + w_1 - x_3 - \tau_l - B_l\dot{\theta}_l^r - J_l\ddot{\theta}_l^r\right), \quad (18)$$

$$\dot{x}_3 = -\alpha\epsilon x_3\left|\frac{w_2}{K_1}\right| - A\epsilon\frac{w_2}{K_1} \quad (19)$$

$$\epsilon\dot{w}_1 = w_2, \quad (20)$$

$$\epsilon\dot{w}_2 = \frac{K_1 Y_p}{J_m}\left\{\frac{J_m}{Y_p J_l}B_l(x_2 + \dot{\theta}_l^r) - \left(\frac{J_m}{Y_p J_l} + Y_p\right)(w_1 - x_3) + \frac{J_m}{Y_p J_l}\tau_l - \frac{J_m\tilde{\theta}''}{Y_p^3}\left(\frac{\epsilon w_2}{K_1} + x_2 + \dot{\theta}_l^r\right)^2 + \tau_{m1}\right\} \quad (21)$$

where $x_1 = \theta_l - \theta_l^r$, $w_1 = z = -K(\theta_l - \frac{\theta_m}{N} + \tilde{\theta}_p)$, $x_3 = q$ and $\epsilon^2 = \frac{K_1}{K}$, and θ_l^r is reference load trajectory to be tracked. Thus f in (11) and g in (12) are given by the right hand sides of (17)-(19) and (20)-(21) respectively. For this singularly perturbed system, the following fact proves that when $\epsilon = 0$, the equation of motion for the rigid case is obtained.

Fact 3.1: With reference to system dynamic equations (17)-(21), when $\epsilon \to 0$, the singularly perturbed flexible system converges to the rigid system given by

$$\left(\frac{J_m}{Y_p^2} + J_l\right)\ddot{\theta}_l + \frac{J_m\tilde{\theta}''}{Y_p^4}\dot{\theta}_l^2 + B_l\dot{\theta}_l + \tau_l = \frac{\tau_{m1}}{Y_p}. \quad (22)$$

proof As $\epsilon \to 0$, $w_2 = 0$ and $w1$ can be solved from (21) as

$$w_1 = \frac{1}{\left(\frac{J_m}{Y_p J_l} + Y_p\right)}\left[\tau_{m1} - \frac{J_m\tilde{\theta}''}{Y_p^3}\left(x_2 + \dot{\theta}_l^r\right)^2 + \frac{J_m}{Y_p J_l}B_l(x_2 + \dot{\theta}_l^r) + \frac{J_m}{Y_p J_l}\tau_l\right] + x_3 \quad (23)$$

Substituting for w_1 in (18) and transforming variables x_1, x_2 to $\theta_l, \dot{\theta}_l$, we get

$$J_l\ddot{\theta}_l + B_l\dot{\theta}_l + \tau_l = \frac{J_l Y_p}{J_m + J_l Y_p^2}\left[\tau_{m1} - \frac{J_m\tilde{\theta}''}{Y_p^3}\dot{\theta}_l^2 + \frac{J_m}{Y_p J_l}(B_l\dot{\theta}_l + \tau_l)\right] \quad (24)$$

Further algebraic simplifications lead to

$$\left(\frac{J_m}{Y_p^2} + J_l\right)\ddot{\theta}_l + \frac{J_m\tilde{\theta}''}{Y_p^4}\dot{\theta}_l^2 + B_l\dot{\theta}_l + \tau_l = \frac{\tau_{m1}}{Y_p}.\square \quad (25)$$

Notice that (25) is same as (3) if we expand τ_{m1}.

IV. CONTROL DEVELOPMENT

The following steps are followed in the development of controller using integral manifold control approach:

1) A composite control law is proposed as $\tau_{m1} = \tau_f + \tau_s$, where τ_f and τ_s are fast and slow control terms, respectively. Fast control τ_f is chosen to make the manifold attractive.
2) With the proposed choice of fast control, the existence of integral manifold h is assured. The manifold needs to satisfy manifold condition (see [14], [15]).
3) For development of the slow control τ_s, polynomial series expansion of integral manifold h ($h = h_0 + h_1\epsilon + h_2\epsilon^2 + ...$) and slow control τ_s ($\tau_s = \tau_0 + \tau_1\epsilon + \tau_2\epsilon^2 + ...$) is used.
4) Using manifold condition, terms of similar power of ϵ are matched to get series of equations for each power of ϵ .
5) Control terms τ_1, τ_2, and so on are chosen such that the infinite series gets truncated. Thus we get a exact expression for control law and for h.

The analysis (refer Appendix-A for details) gives the following controller:

$$\tau_m = B_m\dot{\theta}_m + \tau_f + \tau_0 + \epsilon\tau_1 + \epsilon^2\tau_2 + \epsilon^4\tau_4, \quad (26)$$

$$\tau_f = K_D\epsilon K\left(\dot{\theta}_l - Y_p\dot{\theta}_m\right), \quad (27)$$

$$\tau_1 = K_D\dot{\bar{h}}_0, \quad (28)$$

$$\tau_2 = \frac{J_m\tilde{\theta}''}{Y_p^3}\frac{2(x_2+\theta_l^r)}{K_1}\dot{\bar{h}}_0 + \frac{\ddot{\bar{h}}_0}{C_1}, \quad (29)$$

$$\tau_4 = \frac{J_m\tilde{\theta}''}{Y_p^3}\frac{\bar{\bar{h}}_1^2}{K_1^2}, \quad (30)$$

where,τ_0, and h_0 are given by (50 and (49), respectively. K_D, K_1 are constants and C_1 is given by 48. Simulation results presented in the following section verify the effectiveness of this controller.

V. SIMULATION RESULTS

We define the problem we are addressing in this paper more precisely for simulation purposes as follows. The output position (θ_l) (refer Fig. 3) is required to precisely track a high speed trajectory $\theta_l^r(t) = 10\sin(4\pi t)+25t$ when there is time varying torque load of $\tau_l = 30\sin(2\pi/3t)$ Nm on the output shaft.

To establish the effectiveness of controller designed in the previous section, we compare our results against a controller designed using classically available technique. For comparison if we employ a controller (based on (1)) using output (θ_l) feedback, it is well known that such controllers leads to unstable θ_l in the presence of flexibility which is a part of our hysteresis model. Hence classically known approach (see [16], page 1583 for details) of stabilization in the presence of flexibility is used. The controller used for comparison (without considering KE and hysteresis) is thus given by,

$$\tau_m = B_m\dot{\theta}_m + \tfrac{1}{N}\Big\{(J_l + J_mN^2)(\ddot{\theta}_l^r - \Lambda\dot{e}) + B_l(\dot{\theta}_l^r - \Lambda e) - k_d(\dot{e}+\Lambda e) + \tau_l\Big\} + K_f(\dot{\theta}_l - \tfrac{\dot{\theta}_m}{N}) + \tfrac{\tau_l}{N}. \quad (31)$$

Simulations are carried out with model equations (8)-(10) and the controller given by

1. Equation (26)(See [2] for expanded derivative terms in the control law)
2. Equation (31) for same gains.

Parameters presented in Table II, identified using experimental data, are used in simulation. Results of simulations carried out with and without hysteresis compensation (the known output load is compensated in both the cases) are displayed in Fig. 4-6. Fig. 4 shows the high speed tracking trajectory (along with the load position) and the output load trajectory used in the simulation. Fig. 5 presents the tracking errors in the load and motor positions with and without compensation. We observe clearly that the steady state load position tracking error with hysteresis compensation goes to zero while without compensation goes beyond the encoder resolution. Fig. 6 compares results with full nonlinear model and model used for control development. Compensation 1 (C-1) represents results with model (7) simplified for control development and compensation 2 (C-2) represents results with full nonlinear hysteresis model. We can hardly see difference between results of cases C-1 and C-2 in Fig. 6 in the steady state. The noisy behavior of the error curves in the transient part can be attributed to the numerical implementation of the derivative of the hysteresis state. Thus, the proposed controller achieves successful hysteresis compensation while tracking the output load position. The motor position error is displayed in Fig. 5 to demonstrate that the controller achieves the desired tracking of load position by 'dynamically absorbing' the kinematic error (whatever form it may have) on the motor side. A large motor displacement (from zero) is caused by the controller to compensate for the output load and hysteresis torque.

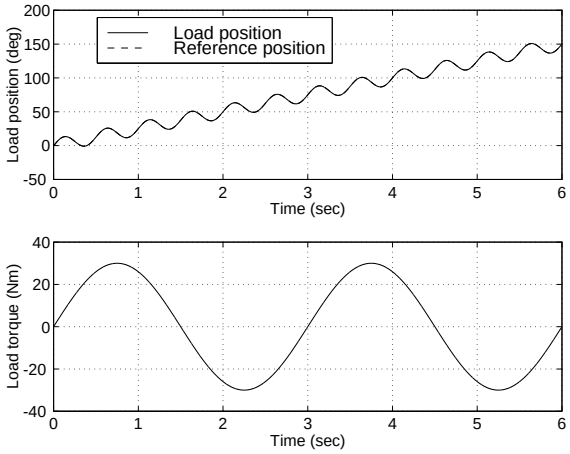

Fig. 4. Tracking and output load trajectories

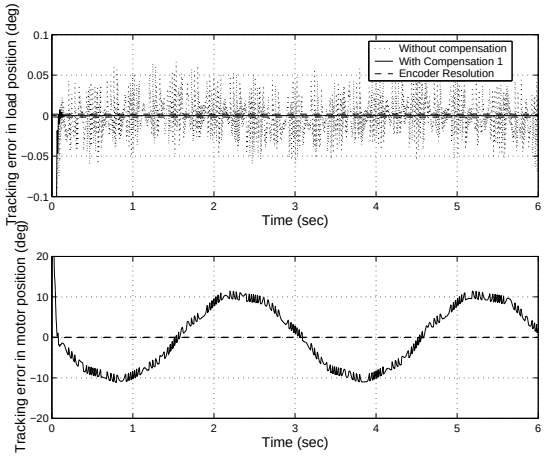

Fig. 5. Tracking errors in the load and the motor position

VI. CONCLUSION

In this paper we presented new control algorithms for compensation of sandwiched hysteresis (with linear flexi-

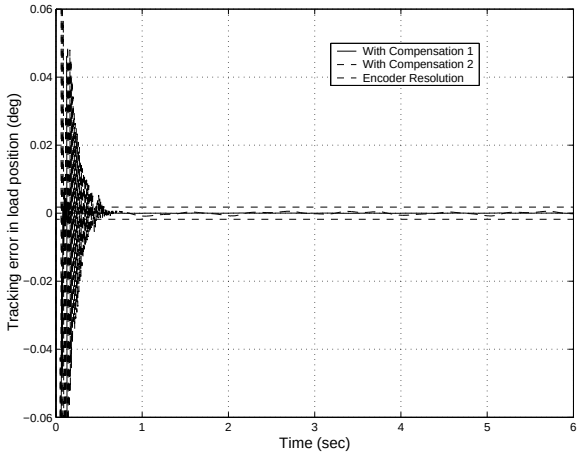

Fig. 6. Tracking errors in the load and the motor position

bility part) in harmonic drives in the presence of kinematic error and smooth output load for high precision tracking applications. The controller is developed using an integral manifold control approach for singularly perturbed systems. Recently developed accurate models of hysteresis and kinematic error in harmonic drives are used. Simulations carried out with the controller and this model verified the effectiveness of the algorithm at compensating for hysteresis and external load. Experimental validation of the proposed algorithm is underway. The proposed control algorithm is useful in high-speed applications to improve the performance of systems using harmonic drives as well as in similar other mechanical systems with sandwiched hysteresis.

ACKNOWLEDGMENTS

This material is partially based upon work supported by the National Science Foundation under Grant No. INT-9819869 and by the Texas Advanced Technology Research Program under grant number TATP 003604-057. Authors also acknowledge reviewers for their constructive comments.

APPENDIX-A

Fast Control

The fast control law τ_f is chosen as

$$\begin{aligned}\tau_f &= -K_D w_2, \\ &= K_D \epsilon K \left(\dot{\theta}_l - Y_p \dot{\theta}_m\right). \end{aligned} \tag{32}$$

With this definition of τ_f, conditions $\mathcal{A}_1$ and $\mathcal{A}_3$ of Lemma 2.1 (existence and properties of integral manifold) in [15] can be easily proved to be satisfied in two different domains given by $w_2 > 0$ and $w_2 < 0$ in the vicinity of h_0. Since conditions $\mathcal{A}_1 - \mathcal{A}_3$ of the lemma are satisfied, there exists $\epsilon_1 \leq \epsilon_0$ such that $\forall \epsilon \in [0, \epsilon_1), \forall \mathbf{x} \in \mathbf{B_x}$ and $\forall \mathbf{w} \in \mathbf{B_w}$, the 5-dimensional system (17)-(21) has a local 2-dimensional integral manifold $\mathcal{M}_\epsilon : \mathbf{w} = h(t, \mathbf{x}, \epsilon) = h_0(t, \mathbf{x}, 0) + H(t, \mathbf{x}, \epsilon)$, and $h(t, \mathbf{x}, \epsilon)$ satisfies the manifold condition:

$$\epsilon \frac{dh}{dt} = g(t, x, h, \epsilon). \tag{33}$$

Note that because the existence conditions are satisfied in two domains, the slow control development is carried out in these two domains separately. However, as we will see later, the control law remains the same in both of these domains.

Slow Control

A slow controller is developed by solving for the manifold condition (33) using power series expansions for τ_s and h in terms of ϵ as mentioned in the development steps above.

Let us expand control law τ_s in powers of ϵ as

$$\tau_s = \tau_0 + \epsilon \tau_1 + \epsilon^2 \tau_2 + \epsilon^3 \tau_3 + \cdots . \tag{34}$$

Similar expansion for the manifold function $h(t, \mathbf{x}, \epsilon)$ is given by

$$h(t, \mathbf{x}, \epsilon) = \begin{bmatrix} \bar{h} \\ \bar{\bar{h}} \end{bmatrix} = \begin{bmatrix} \bar{h}_0 + \epsilon \bar{h}_1 + \epsilon^2 \bar{h}_2 + \cdots \\ \bar{\bar{h}}_0 + \epsilon \bar{\bar{h}}_1 + \epsilon^2 \bar{\bar{h}}_2 + \cdots \end{bmatrix}. \tag{35}$$

Substituting these expressions in the manifold condition (33) and separating terms with similar powers of ϵ, the following sequences of equations are obtained:

$$\begin{aligned} \epsilon^0 : \quad 0 &= \bar{\bar{h}}_0, && (36)\\ \epsilon^1 : \quad \dot{\bar{h}}_0 &= \bar{\bar{h}}_1, && (37)\\ \epsilon^2 : \quad \dot{\bar{h}}_1 &= \bar{\bar{h}}_2, && (38)\\ \epsilon^3 : \quad \dot{\bar{h}}_2 &= \bar{\bar{h}}_3, && (39)\\ &\vdots \end{aligned}$$

and the second set is obtained as

$$\begin{aligned} \epsilon^0 : 0 &= C_1 \left\{ -B_1(x_2 + \dot{\theta}_l^r) - \frac{J_m \tilde{\theta}''}{Y_p^3}(x_2 + \dot{\theta}_l^r)^2 \right. \\ &\quad \left. -J_1 \bar{h}_0 + x_3 + \frac{J_m}{Y_p J_l}\tau_l + \tau_0 \right\}, && (40)\\ \epsilon^1 : 0 &= C_1 \left\{ -K_D \bar{\bar{h}}_1 - J_1 \bar{h}_1 + \tau_1 \right\}, && (41)\\ \epsilon^2 : \dot{\bar{\bar{h}}}_1 &= C_1 \left\{ -\frac{J_m \tilde{\theta}''}{Y_p^3}\frac{2(x_2 + \dot{\theta}_l^r)}{K_1}\bar{\bar{h}}_1 - K_D \bar{\bar{h}}_2 \right. \\ &\quad \left. -J_1 \bar{h}_2 + \tau_2 \right\}, && (42)\\ \epsilon^3 : \dot{\bar{\bar{h}}}_2 &= C_1 \left\{ -\frac{J_m \tilde{\theta}''}{Y_p^3}\frac{2(x_2 + \dot{\theta}_l^r)}{K_1}\bar{\bar{h}}_2 - K_D \bar{\bar{h}}_3 \right. \\ &\quad \left. -J_1 \bar{h}_3 + \tau_2 \right\}, && (43)\\ \epsilon^4 : \dot{\bar{\bar{h}}}_3 &= C_1 \left\{ -\frac{J_m \tilde{\theta}''}{Y_p^3}\left(\frac{\bar{\bar{h}}_1^2}{K_1^2} + \frac{2(x_2 + \dot{\theta}_l^r)}{K_1}\bar{\bar{h}}_3\right) \right. \\ &\quad \left. -J_1 \bar{h}_4 + \tau_4 \right\}, && (44)\\ \epsilon^5 : \dot{\bar{\bar{h}}}_4 &= C_1 \left\{ -\frac{J_m \tilde{\theta}''}{Y_p^3}\left(\frac{2\bar{\bar{h}}_1 \bar{\bar{h}}_2}{K_1^2} + \frac{2(x_2 + \dot{\theta}_l^r)}{K_1}\bar{\bar{h}}_4\right) \right. \\ &\quad \left. -J_1 \bar{h}_5 + \tau_5 \right\}, && (45) \end{aligned}$$

$$\epsilon^6 : \dot{\bar{\bar{h}}}_5 = C_1 \left\{ -\frac{J_m \tilde{\theta}''}{Y_p^3} \left(\frac{\bar{\bar{h}}_2^2 + 2\bar{\bar{h}}_1 \bar{\bar{h}}_3}{K_1^2} - \frac{2(x_2 + \dot{\theta}_l^r)}{K_1} \bar{\bar{h}}_5 \right) - J_1 \bar{h}_6 + \tau_6 \right\}, \quad (46)$$

$$\epsilon^7 : \dot{\bar{\bar{h}}}_6 = C_1 \left\{ -\frac{J_m \tilde{\theta}''}{Y_p^3} \left(\frac{\bar{\bar{h}}_3^2 + 2\bar{\bar{h}}_1 \bar{\bar{h}}_4}{K_1^2} - \frac{2(x_2 + \dot{\theta}_l^r)}{K_1} \bar{\bar{h}}_6 \right) - J_1 \bar{h}_7 + \tau_7 \right\}, \quad (47)$$

$$\vdots$$

where the terms C_1, B_1, and J_1 are defined as follows:

$$\begin{aligned} C_1 &= \frac{K_1 Y_p}{J_m}, \\ B_1 &= -\frac{J_m}{Y_p J_l} B_l, \\ J_1 &= \left(\frac{J_m}{Y_p J_l} + Y_p \right). \end{aligned} \quad (48)$$

The term $\bar{h}_0$ is given from (40) by

$$\bar{h}_0 = \frac{1}{J_1} \left\{ \frac{J_m B_l}{Y_p J_l} (x_2 + \dot{\theta}_l^r) + \frac{J_m}{Y_p J_l} \tau_l - \frac{J_m \tilde{\theta}''}{Y_p^3} (x_2 + \dot{\theta}_l^r)^2 + \tau_0 \right\} + x_3, \quad (49)$$

and the new τ_0 is chosen based on control strategy in [13], [12] as

$$\tau_0 = Y_p \left\{ D(\ddot{\theta}_l^r - \Lambda \dot{e}) + \left(\frac{J_m \tilde{\theta}''}{Y_p^4} \dot{\theta}_l + B_l \right) (\dot{\theta}_l^r - \Lambda e) - k_d (\dot{e} + \Lambda e) + \tau_l \right\}. \quad (50)$$

Notice that $\bar{h}_0$ contains additional terms due to hysteresis ($x_3 = q$) and load τ_l, and τ_0 contains an additional load compensation term τ_l. Slow control law terms τ_1, τ_2, τ_3 and τ_4 are chosen such that the series in ϵ for τ_s and h is truncated. All higher order terms τ_5, τ_6, τ_7 ... are chosen to be zero, to make the corresponding higher order h terms to be zero.

REFERENCES

[1] C. Musser, "Strain Wave Gearing," *United States Patent Number 2,906,143*, 1955.

[2] P. Gandhi, *Modeling and Control of Nonlinear Transmission Attributes in Harmonic Drive Systems*. PhD thesis, Rice University, May 2001.

[3] Harmonic Drive Technologies, Peabody, MA, *http://www.harmonic-drive.com/*.

[4] Harmonic Drive Technologies, Peabody, MA, *HDC Cup Component Gear Set Selection Guide*, 1995.

[5] T. Hidaka, T. Ishida, Y. Zhang, M. Sassahara and Y. Tanioka, "Vibration of a Strain Wave Gearing in an Industrial Robot," in *Proceedings of ASME International Power Transmission and Gearing Conference*, vol. 11, pp. 789, 1989.

[6] T. Tuttle, "Understanding and Modeling the Behavior of a Harmonic Drive Gear Transmission," Master's thesis, Massachussetts Institute of Technology, May 1992. MIT Artificial Intelligence Laboratory Technical Report No. 1365.

[7] N. Kircanski, A. Goldenberg, and S. Jia, "An Experimental Study of Nonlinear Stiffness, Hysteresis, and Friction Effects in Robot Joints with Harmonic Drives and Torque Sensors," in *Proceedings of the 3rd International Symposium on Experimental Robotics*, pp. 327–340, Oct. 1993.

[8] F. Ghorbel, P. S. Gandhi, and F. Altpeter, "On the Kinematic Error in Harmonic Drive Gears," *ASME J of Mechanical Design*, vol. 123, pp. 90–97, Mar. 2001.

[9] P. S. Gandhi and F. Ghorbel, "Modeling, Identification, and Compensation of Friction in Harmonic Drives," in *Proceedings of the 41st IEEE Conference on Decision and Control,Las Vegas, California*, Dec. 2002.

[10] R. Dhaouadi, F. Ghorbel, and P.S. Gandhi, "A new dynamic model of hysteresis in harmonic drives," *IEEE Transactions on Industrial Electronics*, Vol 50 (6), pp. 1165–1171, 2003.

[11] H. K. Tonshoff and J. Kummetz, "Active Compensation of Kinematic Errors in Servo Drives for Machine Tools and Robots," in *American Control Conference, San Diego, CA*, June 1999.

[12] F. Ghorbel and P. Gandhi, "Closed Loop Compensation of Kinematic Error in Harmonic Drives for Precision Control Applications." U.S. Patent No. 6,459,940, Oct. 2002.

[13] P. S. Gandhi and F. Ghorbel, "Closed Loop Compensation of Kinematic Error in Harmonic Drives for Precision Control Applications," *Transactions on Control Systems Technology*, vol. 10, number 6, Nov. 2002.

[14] H. Khalil, *Nonlinear Systems*. Macmillan Publishing Company, New York, 1992. Copublished with Maxwell Macmillan Canada and Maxwell Macmillan International.

[15] F. Ghorbel and M. Spong, "Integral Manifolds of Singularly Perturbed Systems with Applications to Rigid-link Flexible-joint Multibody Systems," *International Journal of Non-Linear Mechanics*, vol. 35, pp. 133–155, 2000.

[16] R. Ortega and M. Spong, "Adaptive motion control of rigid robots: A tutorial," in *Proceedings of the IEEE Conference on Decision and Control,Austin, TX*, pp. 1575–1584, Dec. 1988.